International Journal of Applied Pharmaceutics

ISSN- 0975-7058 Vol 16, Issue 3, 2024

Original Article

MOLECULAR DOCKING DYNAMICS OF SELECTED BENZYLIDENE AMINO PHENYL ACETAMIDES AS TMK INHIBITORS USING HIGH THROUGHPUT VIRTUAL SCREENING (HTVS)

KOPPULA JAYANTHI[1], SYED SUHAIB AHMED[2], MOHD ABDUL BAQI[3], MOHAMMED AFZAL AZAM[1*]

[1]Department of Pharmaceutical Chemistry, JSS College of Pharmacy, JSS Academy of Higher Education and Research, Ooty, Nilgiris, Tamil Nadu, India. [2]Department of Pharmaceutics, JSS College of Pharmacy, JSS Academy of Higher Education and Research, Ooty, Nilgiris, Tamil Nadu, India. [3]Department of Pharmaceutical Biotechnology, JSS College of Pharmacy, JSS Academy of Higher Education and Research, Ooty, Nilgiris, Tamil Nadu, India

*Corresponding author: Mohammed Afzal Azam; *Email: afzal@jssuni.edu.in

Received: 02 Dec 2023, Revised and Accepted: 12 Feb 2024

ABSTRACT

Objective: Thymidylate kinase (TMK) plays a crucial role in bacterial DNA synthesis by catalyzing the phosphorylation of deoxythymidine monophosphate (dTMP) to form deoxythymidine diphosphate (dTDP). Consequently, this enzyme emerges as a promising target for developing novel antibacterial drugs. However, no antibiotics were reported for this target, especially active against *Staphylococcus aureus* thymidylate kinase.

Methods: Benzylidene acetamide-based ligands were examined for their potency using the *in silico* method. These novel ligand structures were built using ChemDraw software. The protein was retrieved from the Research Collaboratory for Structural Bioinformatics Protein Data Bank (RCSB PDB) website. The molecular docking and binding free energy calculation by prime Molecular Mechanics in Generalized Bond Surface Area (MM-GBSA) was performed for selected ligands. A 100 ns molecular dynamic simulation was also performed to assess the stability of the potential ligand as TMK inhibitors.

Results: All ten molecules have shown good glide scores and hydrophobic and hydrogen hydrophobic hydrogen bonding interactions with Arg48, Arg36, and π-π stacking Phe66 in the TMK enzyme (PDB: 4HLC). Among them, N-(2-ethylphenyl)-2-(4-((4-nitrobenzylidene) amino) phenoxy) acetamide molecule had high XP-docking scores of-3.27 kcal/mol based on extra-precision data. Prime Molecular Mechanics in Generalized Bond Surface Area study (MM-GBSA) studies also showed promising binding affinities that are Δ_{Bind} (-65.80), Δ_{Lipo} (-28.55), and Δ_{VdW} (-55.10). Phe66 amino acid residue maintained continuous connections with the ligand during MD simulation. This ligand showed promising binding affinity with the *SaTMK* target.

Conclusion: The N-(2-ethylphenyl)-2-(4-((4-nitrobenzylidene) amino) phenoxy) acetamide ligand at the position of the benzene ring displayed nitrogen and oxygen group, thus indicating good potential activity as the inhibitor of TMK to treat antibacterial agents.

Keywords: Thymidylate kinase (TMK), Molecular docking, Molecular dynamics simulations, MM-GBSA, ADME, HTVS

DOI: https://dx.doi.org/10.22159/ijap.2024v16i3.50023 Journal homepage: https://innovareacademics.in/journals/index.php/ijap

INTRODUCTION

The need for new antibiotics is driven by the recent rise in the incidence of resistance to commonly used antibiotics [1, 2]. The emergence of multiple-drug resistance to commonly-acquired infections, such as those caused by *Staphylococcus aureus*, is particularly alarming due to the ease of transmission in the clinical setup [3, 4]. Clinically, a significant issue associated with *s. aureus* is the remarkable acquisition level of resistance against multiple antibiotic classes, complicating treatment. Despite the antibacterial therapy, *methicillin-resistant S. aureus* (*MRSA*) remains one of the world's most widespread and virulent nosocomial pathogens, causing a significant public health concern [5, 6]. Infections due to *methicillin-resistant* strains of *S. aureus* are associated with higher mortality rates than infections caused by *methicillin-susceptible strains*. In addition, they result in increased lengths of hospital stays and associated healthcare costs [7]. Thus, searching for novel protein targets against which to develop potential anti *s. aureus* drugs have become a priority in antibacterial research. An approach to combat this situation is to discover and develop novel antibiotics with new mechanisms of action. TMK catalyses the phosphorylation of deoxythymidine monophosphate (dTMP) to deoxythymidine diphosphate (dTDP) using ATP as a phosphoryl donor. This step lies at the junction of the *de novo* and *salvage* pathways of thymidine triphosphate (TTP) biosynthesis, which is essential for DNA replication [8]. Thus, TMK is crucial for cell proliferation as well as the survival of the organism. The elucidation of the TMK X-ray structures of both human [9, 10] and *s. aureus* and their low (19%) sequence homology enhances the consideration of TMK as an attractive target for the development of selective inhibitors. Two classes of TMKs have been identified: Class I enzymes are mainly from eukaryotes and have an arginine residue in position x_1 of the consensus sequence $Gxxx_1xGKx$ of the P-loop, which interacts with ATP. Class II TMKs are of prokaryotic origin and can be distinguished by the presence of a glycine residue instead of arginine in the x_1 position of the consensus sequence, along with additional basic residues (mostly Arg) in the LID region that interact with ATP. Inhibitors may thus potentially be designed to specifically target prokaryotic TMKs without affecting the host (human) enzyme, with the expectation that toxicity for the host can be minimized. Inhibitors can be designed targeting the regions of the TMP site conserved between the various bacterial TMKs but with structural differences to that of human thymidine monophosphate kinase (TMK) to obtain broad-spectrum antibacterial agents. The possibility would be to design inhibitors containing hydrogen-bonding groups targeting Arg36, Arg48, and Arg70 at the base of the TMP-binding cavity of Sa*TMK*, an interaction not formed by other TMKs containing proline in this position of the active site and also active Phe66 residue involving transferring phosphate group. In the present work, we aimed to target the charged residues Arg36, Arg48, and Arg70 at the base of the TMP-binding cavity and Phe66 of Sa*TMK* [11]. We have designed 10 benzylidene acetamides such as ((4-chlorobenzylidine)amino)phenoxy)-N-phenylacetamide,(3-chlorophenyl)2-(4-((4-dimethyl-amino)benzylideneamino)phenoxy)acetamide,2-(4-((chlorobenzylidene)amino)phenoxy)-N-phenylacetamide, N-(2-chlorophenyl)-2-(4-((4-(dimethylamino)benzylidene)amino)phenoxy)acetamide, N-(3-bromo phenyl)-2-(4-((3-nitrobenzylidene) amino)phenoxy) acetamide, 2-(4-((2,4-dichlorobenzylidene)amino)phenoxy)-N-mesitylacetamide, N-(2-ethylphenyl)-2-(4-((4-nitrobenzylidene) amino) phenoxy)acetamide 2-(4-((2,4-dichloro-benzylidene)

amino)phenoxy)-N-phenylacetamide, N-(3-chlorophenyl)-2-(4-((4-nitrobenzylidene)amino)phenoxy)acetamide,2-(4-((4-chlorobenzylidene)amino)phenoxy)-N-(3-chlorophenyl)acetamide and were depicted in specified codes for these compounds as BP02, BP10, BP22, BP25, BP14, BP13, BP16, BP03, BP06 and BP07. No reports were available for these identified compounds as specific inhibitors of the *SaTMK* target. However, sulfonylpiperidines exhibited inhibitory activity against bacterial TMK. They have reported and documented the interactions of sulfonylpiperidines with Arg70, Arg48, Ser97, Gln101, and Phe66, thereby resulting in notable *in vitro* enzyme inhibition activities against Gram-positive pathogens, including *S. pneumoniae* (IC_{50}, 0.5 nm) and *s. aureus* (IC_{50}, 0.5 nm) [12]. These compounds also exhibited promising antibacterial activity against these two tested strains. Earlier reports suggest that they have targeted different bacteria TMKs with different compounds. All those compounds followed Lipinski's rules (MW<350g/mol) [13, 14] for the *mycobacteria* TMK PDB: 5NQ5 binding energy was found to be-36.75kal/mol. After docking essential amino acids for docked compound tetrahydro pyrimidinone Arg95, Arg107, Asn100 Arg75 with hydrogen bonds [15]. In the present study, there were no reports found specifically for *SaTMK.* Hence, we specifically aimed to target *SaTMK* to identify novel compounds as antibacterial agents that could have less chance to develop resistance. We expect that benzylidene acetamide-based derivatives would also exhibit promising results in *in vitro* activity against *SaTMK*, as these compounds have high binding affinity against the specified target.

MATERIALS AND METHODS

Molecular docking

Energy, score, and e-model values determined the optimal docked attitude for every ligand. A computer technology known as molecular docking has been utilized for predicting the ligand's binding mechanism and affinity for the target. The docked conformers were tuned depending on the system's total energy [16, 17]. The *X-ray* crystal structure of *S. aureus* TMK (PDB: 4HLC, resolution: 1.55Å) was chosen for the modelling effort [12]. Schrödinger suite 2019-2, preparation of the izard module was used to prepare the protein [18]. The addition of hydrogen destroyed the crystallographic water molecules [19]. Prime (Schrödinger suite 2019-2) accommodated the missing side chain. The OPLS3e forcefield was employed to reduce energy consumption while maintaining the root mean square deviations (RMSD) of heavy atoms at 0.30 molar [20]. The active site was characterized by a radius of ten around the bound ligand in a grid box with the co-crystallized ligand in the middle. Glide was used to dock the 10 ligands synthesized with LigPrep in extra-precision (XP) mode, with all other settings left at their default. Glide energy, score, and e-model values determined the optimal docked attitude for every ligand.

Binding free energy calculations using prime MM-GBSA

The binding free energy for each protein-ligand combination was calculated using the prime Molecular Mechanics-Generalized Born Surface Area (MM-GBSA) approach (Schrödinger suite 2019-2). An OPLS3e force field with a VSGB 2.0 solvation model was used for energy minimization [21, 22]. This technique contains optimal implicit solvation for hydrogen bonding, self-contact interaction interactions, and hydrophobic interactions, in addition to a physics-based correction.

Molecular dynamics simulation

Time-step methods were used in the reference system propagator algorithm for bonded electrostatic forces, which can be non-bonded, short-range or long-range. Every 100 PS, data was collected and trajectories were analyzed [23]. We have performed MD simulation using (Schrödinger suite 2019-2), investigated top-ranked compound's nuclear binding behavior, and understood molecular interfaces [24]. To solve the complex BP16/4HLC, the TIP4P water model with orthorhombic periodic borders and a buffer zone of 10 between Protein atoms and box edges was employed [25]. To neutralize the generated system 0.15 molar, NaCl counter ions were provided Energy was minimized using the OPLS3eforce field adjustments. Long-range electrostatic interactions were calculated with a tolerance of 1e-09 utilizing the Ewald smooth particle mesh method [26]. The short-range Vander Waals and Coulomb interactions were estimated at a cut-off radius of 9.0. One hundred ns of MD simulations at two fs per time step were done at 300 Kelvin and 1 bar of pressure in an isothermal-isobaric ensemble [Simulation of a system with constant number (N) and constant temperature (T), but variable pressure (P)]. At 100 and 200 PS, The Nose-Hoover thermostat chain thermostat and Martyna-Tobias-Klein barostat techniques are integrated [27, 28]. Multiple time-step methods were used in the reference system propagator algorithm for bonded electrostatic forces, which can be non-bonded, short-range or long-range. Every 100 PS, data was collected, and trajectories were analyzed.

RESULTS AND DISCUSSION

Molecular docking and binding free energy calculations

It can be seen from fig. 1 that most of the designed compounds occupied the thymidine monophosphate (TMP)-binding site of *SaTMK*, located at the interface of N-and central domains of the catalytic pocket. This is in agreement with earlier studies where co-crystallized inhibitors occupied the same binding site [10, 29]. It is also evident that these compounds formed hydrogen bonding interactions mainly with the charged and polar residues of the N-terminal domain. Hydrogen bonding interactions were observed with conserved Arginine triad, Arg36, Arg48, and Arg92 of catalytic pocket. This result is in correlation with the sulfonyl piperidine compounds co-crystallized with *S. aureus* TMK [12]. In most of the compounds, hydrogen bonding interaction was also observed with charged residue Glu37. Except for BP16, all other compounds exhibited π-π stacking interaction with the phenyl ring of Phe66. This lucrative hydrophobic interaction further enhanced the stability of these compounds in the catalytic pocket. Using the *SaTMK* (PDB: 4HLC), we have validated docking protocols by using the MM-GBSA incorporated in Schrodinger Suite 2019-2. The co-crystallized bound ligand conformational Orientation was identical to the docking pose with an RMSD of 1.01 Å. This docking protocol used a virtual screening approach to remove the functional groups that interact with ligands using Lipinski's rule; XP-docking results in glide score, e-model, evdw, ecoul, and energy. All compounds have physicochemical parameters of fragments (MW<500 g/mol) or lead compound BP16 (MW<403.44 g/mol) that follow Lipinski's rule, which could lead to a potent compound for further development [13].

Table 1: The XP-docking score of compounds of 1-10 in the catalytic pocket of (PDB: 4HLC) thymidylate kinase (kcal/mol)

S. No.	Compound code	[a]Gscore	[b]Gemodel	[c]Gevdw	[d]Gecoul	[e]Genergy
1	BP02	-4.76	-59.47	-36.47	-3.18	-39.65
2	BP03	-3.03	-58.46	-39.34	-4.36	-43.70
3	BP06	-2.80	-61.21	-42.31	-3.23	-45.54
4	BP07	-2.68	-66.34	-44.66	-1.14	-45.81
5	BP10	-4.61	-62.54	-36.50	-3.43	-39.93
6	BP13	-3.60	-52.29	-35.42	-0.25	-35.68
7	BP14	-3.76	-60.60	-45.42	-1.50	-49.93
8	BP16	-3.27	-56.35	-38.07	-1.12	-39.19
9	BP22	-4.51	-61.98	-36.88	-2.89	-39.78
10	BP25	-4.36	-62.51	-43.06	0.02	-43.03

[a]glide score; [b]glide model energy; [c]glide van der Waals energy; [d]glide Coulomb energy; [e]glide energy.

The docking results depicted in table 1 showed that all ligands have at least one hydrogen bond with amino acids and the best glide scores from -4.76 to-2.68 kcal/mol. In the XP-docking BP02 BP10, these two compounds showed high glide scores of-4.76 to-4.61 kcal/mol, respectively, while compound BP16 showed glide scores of-3.27 kcal/mol. Further, binding free energies (Δ_{Bind}) of the selected hits top-scoring poses were computed (-60.62 to -84.42 kcal/mol) by the MM-GBSA approach.

Table 2: **Contribution of binding free energy (MM-GBSA) (kcal/mol) between selected 10 compounds and thymidylate kinase (PDB: 4HLC)**

S. No.	Compound code	[a]ΔG_{Bind}	[b]ΔG_{Coul}	[c]ΔG_{HB}	[d]ΔG_{Lip}	[e]ΔG_{VdW}
1	BP02	-72.28	-15.11	-2.04	-33.53	-46.44
2	BP10	-65.00	-35.27	-3.21	-20.79	-49.38
3	BP22	-63.68	-23.05	-1.34	-29.92	-55.81
4	BP25	-61.47	-36.70	-0.09	-22.76	-54.35
5	BP14	-71.10	-26.88	-2.89	-29.18	-61.97
6	BP13	-84.42	-30.30	-4.47	-23.53	-62.57
7	BP16	-65.80	-32.18	-1.31	-28.55	-55.10
8	BP03	-60.62	-7.72	-0.97	-30.69	-37.31
9	BP06	-61.69	-27.58	-1.75	-33.84	-42.83
10	BP07	-60.95	-24.84	-2.68	-31.80	-45.40

Free energy of binding; [b]Coulomb energy; [c]hydrogen bonding energy; [d]hydrophobic energy (non-polar contribution estimated by solvent accessible surface area);[e]vander Waals energy.

In table 2, the considerable Vander Waal energy (ΔG_{VdW}) ranges from -37.31 to-62.57 kcal/mol and strongly favoured the binding to the target protein. On the other hand, the hydrophobic energy term (ΔG_{Lipo}) ranged from -20.79 to-33.84 kcal/mol and moderately favoured the binding. It is also evident that the Coulomb energy term (ΔG_{Coul},-7.72 to-36.70 kcal/mol) is moderately favourable for the binding of selected compounds. The BP02 and BP10 got the most excellent glide scores ranging from -4.76 and -4.61 kcal/mol, respectively. The compounds BP02 and BP13 showed the highest binding affinity with -72.28 and -84.42 kcal/mol, respectively, according to the MM-GBSA-based binding free energy calculation. The data reveals that benzylidene acetamide-based derivatives BP16 demonstrate a binding energy of-65.80 kcal/mol with *S. aureus* thymidylate kinase (*SaTMK,* PDB: 4HLC), specifically interacting with Arg36, Arg48, Arg92, and Phe66. This is in contrast to a lower binding energy (-36.75 kcal/mol) observed for tetrahydro pyrimidinone derivatives with *Mycobacterium tuberculosis* thymidylate kinase (*MTBTMK*, PDB: 5NQ5), involving Arg95, Arg75, Arg107, Asn100 [15]. Given this higher affinity of BP16 for *SaTMK*, these compounds emerge as promising candidates for developing inhibitors against *s. aureus* infections. 2D interactions for all ten compounds are shown in fig. 1.

Comp. code	Structure	2D-interaction
BP02	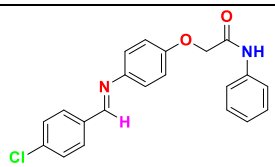	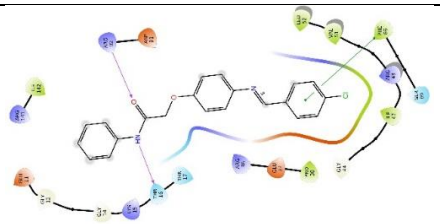
BP03	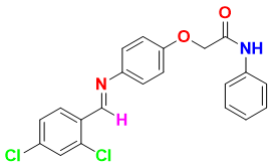	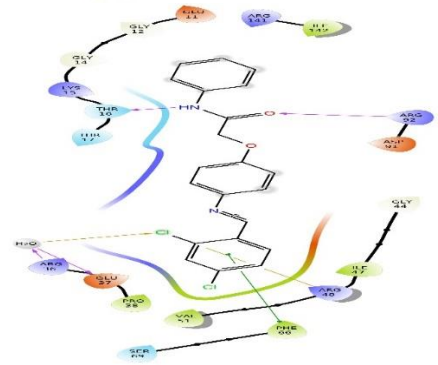
BP06	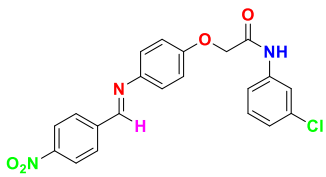	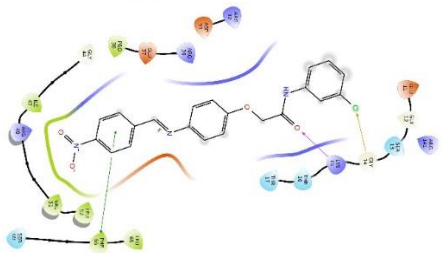

Comp. code	Structure	2D-interaction
BP07	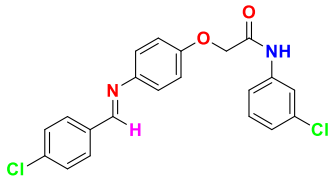	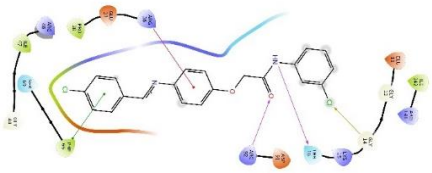
BP10	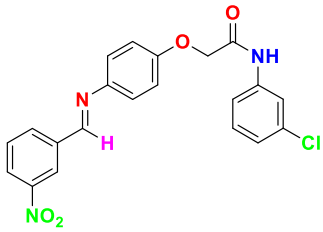	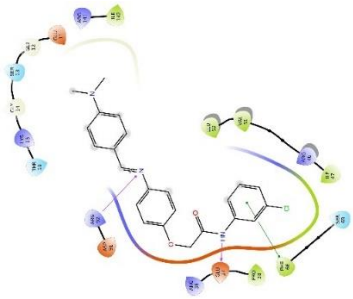
BP13	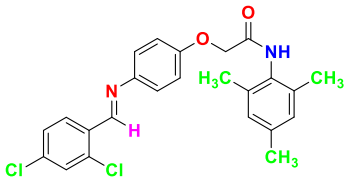	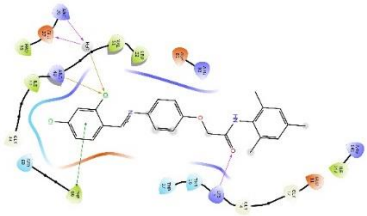
BP14	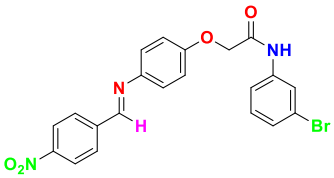	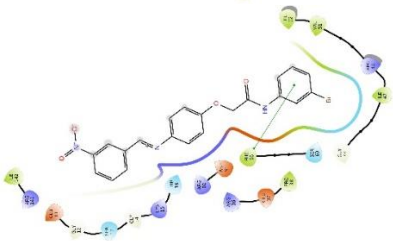
BP16	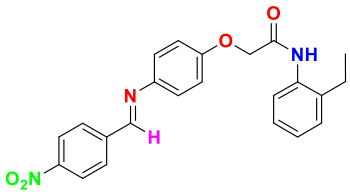	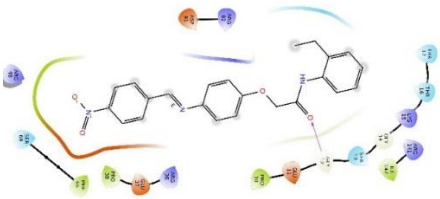
BP22	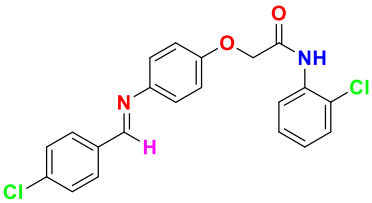	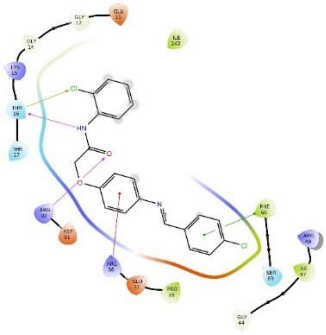
BP25	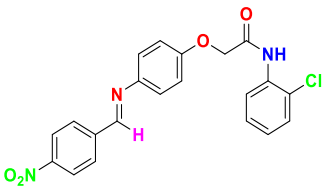	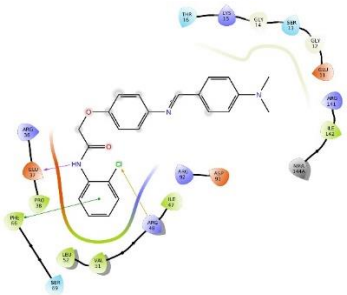

Fig. 1: 2D-interaction diagrams of ten designed compounds in the catalytic pocket of *Sa*TMK (PDB: 4HLC)

Table 3: The number of hydrogen bonds and interacting amino acid residues for selected ten hits in the TMK catalytic pocket (PDB: 4HLC)

S. No.	Compound code	Number of hydrogen bonds	Interacting amino acid residues
1	BP02	2	THR16, ARG92
2	BP03	3	GLU37, ARG92, THR16
3	BP06	1	LYS15
4	BP07	2	THR16, ARG92
5	BP16	1	GLY12
6	BP10	2	ARG92, GLU37
7	BP13	3	ARG36, GLU37, LYS15
8	BP14	0	-
9	BP22	2	THR16, ARG92
10	BP25	1	GLU37

Table 3 indicates hydrogen bonding interactions with amino acid residues for designed molecules. It was chosen for further investigation by considering both the docking score and binding affinity stability compared to BP02 and BP13, which do not retain docking and glide bind stability. Sometimes, one is higher than the other. However, BP16 has a considerably higher glide score and glide energy. Therefore, we underwent further investigation for the molecular dynamics (MD) simulation study of BP16 with *s. aureus* TMK protein.

MD simulation study

The ligand N-(2-ethylphenyl)-2-(4-((4-nitrobenzylidene) amino) phenoxy) acetamide, BP16/4HLC docked pose was used to run a 100 ns of molecular dynamic simulations. During simulation, root mean square deviations (RMSD) of all Cα atoms increased up to 40 ns and then stabilized in the range of 1.56 to 2.71 Å, indicating the low conformational flexibility of protein during simulation (fig. 2). Except for the loop region, root mean square fluctuations (RMSF) of residues binding to the ligand fluctuated between 0.56 to 2.59 Å (fig. 3), further indicating the less changes in protein structure during simulation. Protein-ligand interactions fraction diagram (fig. 4) and protein-ligand contacts timeline (fig. 5 and fig. 6) indicate that ligand-protein interactions, dominated by direct and via water-bridged hydrogen bonds, are mainly with residues lying in the region Glu11 to Tyr100 of N-terminal and the central domain of catalytic pocket protein-ligand. During simulation, BP16 formed strong hydrogen bonding interaction with charged residue Glu37 (~62% of MD simulation) and intermediate frequency interactions with Glu11, Glu37, Arg48, Leu52, Ser69, Arg70, His 73, and Arg92 (fig. 5 and fig. 6). This compound also exhibited strong hydrophobic π-π stacking with Phe66 (~90% of MD simulation) and intermediate frequency π-π stacking interactions with Pro38, Ile47, Val51, and Leu52. It is evident from the above result that apart from hydrogen bonding interactions, hydrophobic interactions are also important for the stability of ligand BP16 in the catalytic pocket.

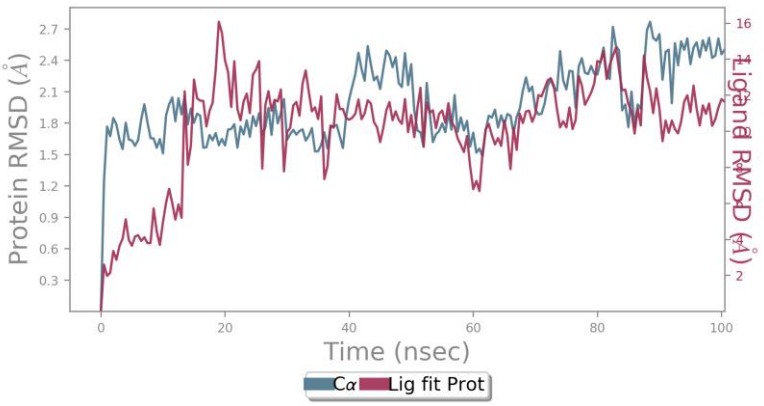

Fig. 2: The plot represents the RMSD of Cα atoms during the MD simulation of the BP16/4HLC complex

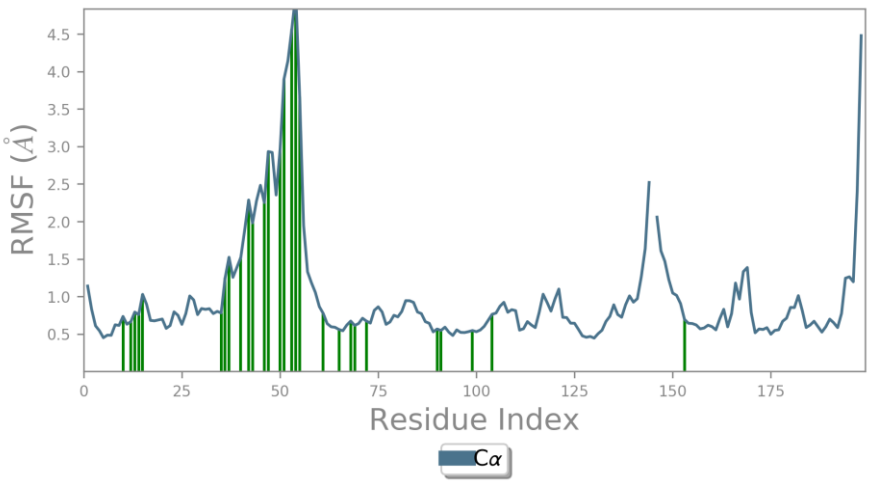

Fig. 3: Represents RMSF plot of BP16/4HLC complex during MD simulation

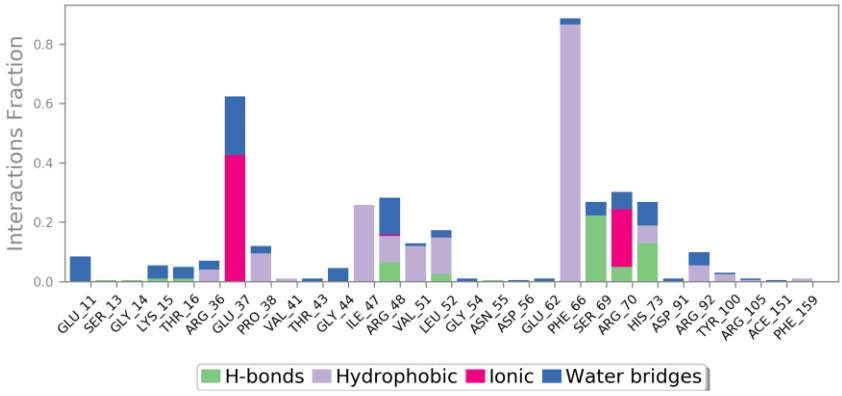

Fig. 4: Protein-ligand contacts profile for BP16/4HLC complex during MD simulation trajectory

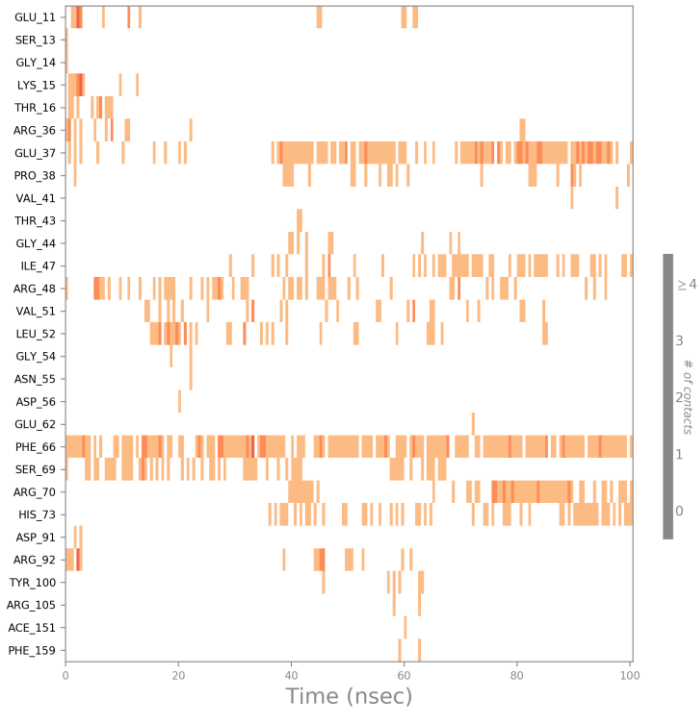

Fig. 5: Timeline representation of BP16/4HLC complex during simulation trajectory

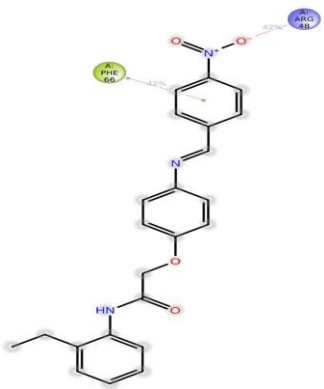

Fig. 6: 2D diagram for BP16/4HLC complex

Phe66 maintained continuous contact with the aromatic ring with π-π, stating the bond stable at 42%, and Arg48 claimed the connections with the oxygen group with multiple bonds and steady at 42% in the particular studies. In the overall view, the ligand BP16 showed good activity for developing the new *SaTMK* inhibitors.

CONCLUSION

In this study, compounds were selected particularly to target *SaTMK*. In this, the presence of an oxygen group was found essential to retain the inhibitory activity of compound BP16. According to the docking studies, it was found that all 10 compounds showed good binding affinity towards *SaTMK*. Most of the compounds exhibited hydrogen bonding interactions with the conserved Arginine triad, Arg36, Arg48 and Arg92 of the catalytic pocket. These compounds also showed π-π stacking with the phenyl ring of Phe66. Among them, N-(2-ethyl phenyl)-2-(4-((4-nitro benzylidene) amino) phenoxy) acetamide showed high negative values of Δ_{Bind}-65.80 kcal/mol), Δ_{VdW} (-55.10 kcal/mol) and Δ_{Lipo} (-28.55 kcal/mol) in binding free energy calculation by MM-GBSA approach. Further, this novel-designed ligand showed protein-ligand contacts with the Arg36, Arg48, and Phe66 amino acid residues and maintained continuous connections with protein during MD simulation. BP16 followed the Lipinski rule (MW<403.44 g/mol). We interpreted the

data with previous studies, targeting *MTBTMK* using tetrahydro pyrimidinone derivatives, achieving a binding energy of-36.75 Kcal/mol. In comparison, benzylidene acetamide-based derivatives exhibited higher binding energy (-65.80 Kcal/mol) with *SaTMK* compared to the previous docking data with *MTBTMK*. Targeting of *SaTMK* benzylidene acetamide-based derivates has shown hydrogen bonding interactions mainly with polar residues of the N-terminal domain and Hydrogen bonding interactions were observed with conserved arginine triad, Arg36, Arg48, and Arg92 of catalytic pocket. This result is in correlation with the sulfonyl piperidine compounds co-crystallized with *S. aureus* TMK. Targeting *SaTMK* with benzylidene acetamide-based derivatives presents a promising avenue for developing antibacterial agents, given their favourable binding affinities and interaction with Arg48. The presence of oxygen further enhances their potential for potent *in vitro* activity, suggesting a novel approach for future studies.

ACKNOWLEDGMENT

The authors would like to thank the Department of Pharmaceutical Chemistry, JSS College of Pharmacy, Ooty, Tamil Nadu for providing facilities for conducting Research.

FUNDING

No funding was received for this work.

AUTHORS CONTRIBUTIONS

Koppula Jayanthi-Conceptualization, validation, writing-original draft preparation, and Data curation. Syed Suhaib Ahmed-Data curation, methodology, writing-Review and Editing. Mohd Abdul Baqi-Data curation, writing, and editing. Mohd Afzal Azam-Conceptualization, Formal analysis, validation, and supervision.

CONFLICT OF INTERESTS

There is no conflict of interest

REFERENCES

1. Jones TF, Creech CB, Erwin P, Baird SG, Woron AM, Schaffner W. Family outbreaks of invasive community-associated methicillin-resistant staphylococcus aureus infection. Clin Infect Dis. 2006;42(9):e76-8. doi: 10.1086/503265, PMID 16586378.
2. Bhatia R, Narain JP. The growing challenge of antimicrobial resistance in the South-East Asia Region–are we losing the battle? Indian J Med Res. 2010;132(5):482-6. doi: 10.4103/0971-5916.73313, PMID 21149995.
3. Shurland S, Zhan M, Bradham DD, Roghmann MC. Comparison of mortality risk associated with bacteremia due to methicillin-resistant and methicillin-susceptible staphylococcus aureus. Infect Control Hosp Epidemiol. 2007;28(3):273-9. doi: 10.1086/512627, PMID 17326017.
4. Moran GJ, Krishnadasan A, Gorwitz RJ, Fosheim GE, McDougal LK, Carey RB. Methicillin-resistant *s. aureus* infections among patients in the emergency department. N Engl J Med. 2006 Aug 17;355(7):666-74. doi: 10.1056/NEJMoa055356, PMID 16914702.
5. Lakhundi S, Zhang K. Methicillin-resistant staphylococcus aureus: molecular characterization, evolution, and epidemiology. Clin Microbiol Rev. 2018 Oct;31(4):e00020-18. doi: 10.1128/CMR.00020-18, PMID 30209034.
6. Khan TM, Kok YL, Bukhsh A, Lee LH, Chan KG, Goh BH. Incidence of Methicillin-Resistant Staphylococcus Aureus (MRSA) in burn intensive care unit: a systematic review. GERMS. 2018;8(3):113-25. doi: 10.18683/germs.2018.1138, PMID 30250830.
7. Antonanzas F, Lozano C, Torres C. Economic features of antibiotic resistance: the case of methicillin-resistant staphylococcus aureus. Pharmacoeconomics. 2015 Apr;33(4):285-325. doi: 10.1007/s40273-014-0242-y, PMID 25447195.
8. Munier Lehmann H, Chaffotte A, Pochet S, Labesse G. Thymidylate kinase of mycobacterium tuberculosis: a chimera sharing properties common to eukaryotic and bacterial enzymes. Protein Sci. 2001 Jun;10(6):1195-205. doi: 10.1110/ps.45701, PMID 11369858.
9. Ostermann N, Schlichting I, Brundiers R, Konrad M, Reinstein J, Veit T. Insights into the phosphoryl transfer mechanism of human thymidylate kinase gained from crystal structures of enzyme complexes along the reaction coordinate. Structure. 2000;8(6):629-42. doi: 10.1016/s0969-2126(00)00149-0, PMID 10873853.
10. Kotaka M, Dhaliwal B, Ren J, Nichols CE, Angell R, Lockyer M. Structures of *s. aureus* thymidylate kinase reveal an atypical active site configuration and an intermediate conformational state upon substrate binding. Protein Sci. 2006 Apr;15(4):774-84. doi: 10.1110/ps.052002406, PMID 16522804.
11. Jayanthi K, Azam MA. Thymidylate kinase inhibitors as antibacterial agents: a review. Appl Biochem Microbiol. 2023 Jun;59(3):250-66. doi: 10.1134/S0003683823030092.
12. Martinez Botella G, Loch JT, Green OM, Kawatkar SP, Olivier NB, Boriack Sjodin PA. Sulfonylpiperidines as novel, antibacterial inhibitors of gram-positive thymidylate kinase (TMK). Bioorg Med Chem Lett. 2013;23(1):169-73. doi: 10.1016/j.bmcl.2012.10.128, PMID 23206863.
13. Lipinski CA. Lead and drug-like compounds: the rule-of-five revolution. Drug Discov Today Technol. 2004;1(4):337-41. doi: 10.1016/j.ddtec.2004.11.007, PMID 24981612.
14. Pham EC, Thi TVL, Phan LT, Nguyen HT, Le KNB, Truong TN. Design, synthesis, antimicrobial evaluations and *in silico* studies of novel pyrazol-5(4H)-one and 1H-pyrazol-5-ol derivatives. Arab J Chem. 2022 Mar 1;15(3):103682. doi: 10.1016/j.arabjc.2021.103682.
15. Venugopala KN, Tratrat C, Pillay M, Chandrashekharappa S, Al-Attraqchi OHA, Aldhubiab BE. *In silico* design and synthesis of tetrahydropyrimidinones and tetrahydropyrimidinethiones as potential thymidylate kinase inhibitors exerting anti-tb activity against mycobacterium tuberculosis. Drug Des Devel Ther. 2020 Mar;14:1027-39. doi: 10.2147/DDDT.S228381, PMID 32214795.
16. James JP, Aiswarya TC, Priya S, Jyothi D, Dixit SR. Structure-based multitargeted molecular docking analysis of pyrazole-condensed heterocyclics against lung cancer. Int J App Pharm. 2021;3(6):157-69. doi: 10.22159/ijap.2021v13i6.42801.
17. Dar AM, Mir S. Molecular docking: approaches, types, applications and basic challenges. J Anal Bioanal Tech. 2017;8(2):1-3. doi: 10.4172/2155-9872.1000356.
18. Sastry GM, Adzhigirey M, Day T, Annabhimoju R, Sherman W. Protein and ligand preparation: parameters, protocols, and influence on virtual screening enrichments. J Comput Aided Mol Des. 2013 Mar;27(3):221-34. doi: 10.1007/s10822-013-9644-8, PMID 23579614.
19. Sukumaran S, MM, SS, BA, SS, S ST. In silico analysis of acridone against TNF-α and PDE4 targets for the treatment of psoriasis. Int J Res Pharm Sci. 2020 Dec 18;11(4):7790-8.
20. Dunkel M, Fullbeck M, Neumann S, Preissner R. Supernatural: a searchable database of available natural compounds. Nucleic Acids Res. 2006;34:D678-83. doi: 10.1093/nar/gkj132, PMID 16381957.
21. Jacobson MP, Pincus DL, Rapp CS, Day TJF, Honig B, Shaw DE. A hierarchical approach to all-atom protein loop prediction. Proteins. 2004 May;55(2):351-67. doi: 10.1002/prot.10613, PMID 15048827.
22. Dhawale S, Gawale S, Jadhav A, Gethe K, Raut P, Hiwarale N. *In silico* approach targeting polyphenol as Fabh inhibitor in bacterial infection. Int J Pharm Pharm Sci. 2022;14(11):25-30. doi: 10.22159/ijpps.2022v14i11.45816.
23. Martyna GJ, Tuckerman ME, Tobias DJ, Klein ML. Explicit reversible integrators for extended systems dynamics. Mol Phys. 1996;87(5):1117-57. doi: 10.1080/00268979600100761.
24. Guo Z, Mohanty U, Noehre J, Sawyer TK, Sherman W, Krilov G. Probing the α-helical structural stability of stapled p53 peptides: molecular dynamics simulations and analysis. Chem Biol Drug Des. 2010 Apr;75(4):348-59. doi: 10.1111/j.1747-0285.2010.00951.x, PMID 20331649.
25. Essmann U, Perera L, Berkowitz ML, Darden T, Lee H, Pedersen LG. A smooth particle mesh ewald method. J Chem Phys. 1995;103(19):8577-93. doi: 10.1063/1.470117.
26. Harder E, Damm W, Maple J, Wu C, Reboul M, Xiang JY. OPLS3: A force field providing broad coverage of drug-like small

molecules and proteins. J Chem Theory Comput. 2016 Jan 12;12(1):281-96. doi: 10.1021/acs.jctc.5b00864, PMID 26584231.

27. Martyna GJ, Tobias DJ, Klein ML. Constant pressure molecular dynamics algorithms. J Chem Phys. 1994 Sep 1;101(5):4177-89. doi: 10.1063/1.467468.
28. Badavath VN, Sinha BN, Jayaprakash V. Design, *in silico* docking and predictive ADME properties of novel pyrazoline derivatives with selective human MAO inhibitory activity. Int J Pharm Pharm Sci. 2015;7:277-82.
29. Haouz A, Vanheusden V, Munier Lehmann H, Froeyen M, Herdewijn P, Van Calenbergh S. Enzymatic and structural analysis of inhibitors designed against mycobacterium tuberculosis thymidylate kinase. New insights into the phosphoryl transfer mechanism. J Biol Chem. 2003;278(7):4963-71. doi: 10.1074/jbc.M209630200, PMID 12454011.